agriculture

MDPI

Article

Detection and Differentiation between Laurel Wilt Disease, Phytophthora Disease, and Salinity Damage Using a Hyperspectral Sensing Technique

Jaafar Abdulridha, Reza Ehsani * and Ana de Castro

Citrus Research and Education Center, University of Florida, 700 Experiment Station Rd., Lake Alfred, FL 33850, USA; jafar.rida@yahoo.com (J.A.); anadecastro80@gmail.com (A.d.C.)

* Correspondence: ehsani@ufl.edu; Tel.: +1-863-956-8770; Fax: +1-863-956-4631

Academic Editor: Ritaban Dutta

Received: 1 August 2016; Accepted: 9 October 2016; Published: 27 October 2016

Abstract: Laurel wilt (Lw) is a fatal disease. It is a vascular pathogen and is considered a major threat to the avocado industry in Florida. Many of the symptoms of Lw resemble those that are caused by other diseases or stress factors. In this study, the best wavelengths with which to discriminate plants affected by Lw from stress factors were determined and classified. Visible-near infrared (400–950 nm) spectral data from healthy trees and those with Lw, Phytophthora, or salinity damage were collected using a handheld spectroradiometer. The total number of wavelengths was averaged in two ranges: 10 nm and 40 nm. Three classification methods, stepwise discriminant (STEPDISC) analysis, multilayer perceptron (MLP), and radial basis function (RBF), were applied in the early stage of Lw infestation. The classification results obtained for MLP, with percent accuracy of classification as high as 98% were better than STEPDISC and RBF. The MLP neural network selected certain wavelengths that were crucial for correctly classifying healthy trees from those with stress trees. The results showed that there were sufficient spectral differences between laurel wilt, healthy trees, and trees that have other diseases; therefore, a remote sensing technique could diagnose Lw in the early stage of infestation.

Keywords: Laurel wilt; spectroradiometer; hyperspectral classification; remote sensing; multilayer perceptron

1. Introduction

Avocado is the second most important tropical fruit crop in Florida after citrus [1] valued at tens of millions of dollars per year [2,3]. The avocado crop is valuable to the state economy, and the avocado industry brings in a substantial amount of "new dollars" to the state, resulting in an overall economic impact of close to $100 million per annum [3]. However, the revenue from avocado in Florida has been greatly reduced (by 50%) due to the effects of laurel wilt (Lw) disease [3,4]. Lw disease has caused serious losses in fruit quality and quantity, resulting in reduced sales, as well as an increase in agro-industrial waste, pesticide costs, and management expenses [4]. Lw disease has been reported as a major threat to the commercial production of avocado in Florida [5,6]. One vector of Lw disease is the redbay ambrosia beetle [3,4,7,8]. The redbay ambrosia beetle, *Xyleborus glabratus Eichhoff* (Coleoptera, Curculionidae, Scolytinae) is associated with fungal symbionts such as *Raffaelea lauricola* [9,10], a fungus that kills the tree by blocking water flow to the canopy [11].

The secretion of redbay ambrosia beetle saliva helps to spread *R. lauricola* from tree to tree [12]. In addition, *R. lauricola* grows rapidly inside the wooden stems [5,13]. The fungi reduce the tree's ability to transfer nutrients and water to the branches and leaves. Generally, the disease causes several changes to the plant, such as the change in color of the leaves from green to a red-purple brown,

the underside of the bark becomes black, and small pores and holes form inside the outermost layer of bark [14]. All of these symptoms may indicate the presence of the redbay ambrosia beetle in the tree [9,14]. Many of the disease symptoms are similar to those caused by other diseases such as Phytophthora root rot (*Phytophthora cinnamomi*) or factors such as lightning damage, freeze damage, or drought stress [15], making visual detection of Lw difficult. Moreover, the development of external symptoms signifies colonization of the host [16]. It may not be possible to manage the disease once plants display external symptoms [17]. Therefore, an advanced and rapid method for detecting Lw that can distinguish these biotic and abiotic stresses is needed [18]. Currently, the only method to reduce the effect of Lw is by complete removal of the infected tree, including the root, so that vectors cannot transfer the disease to healthy trees [2,10,15]. Lw disease has spread very quickly in just a few years through Florida and other states [16], so it is necessary to find a rapid method to detect the disease in a timely manner to at least reduce the spread of the redbay ambrosia beetle. There are several methods that can detect the disease, such as scouting and polymerase chain reaction (PCR) [19], but they are costly and time consuming; therefore, it would be helpful to develop a faster and more rapid method of detecting Lw disease [20]. Spectral reflectance is a method that is considered to be rapid and non-destructive [21]. Spectral reflectance methods depend on reflected or emitted radiation from different bodies, so each material has a different spectral signature [22,23]. For plant signatures, the spectral reflectance either increases or decreases depending on physical (external) factors such as chlorophyll and pigment concentration which are used as indicators of the plant condition in the visible range (450–760 nm) [24–26]. There are also other factors such as physiological structure, condition of the cell wall, water content, surface roughness, and stoma activity which will affect light penetration through the leaf structure, so the spectral signature in the near infrared (NIR) range of 760 to 2500 nm is used to indicate these factors [27,28].

It is possible to use Visible-Near Infrared (V-NIR) techniques to distinguish healthy from unhealthy leaves [26,29–31]. Ma et al. [32] used a visible remote sensor with different multi-spectral wavelengths to detect citrus greening. Some studies confirmed that spectrometric methods are more effective, more accurate, less time-consuming, and nondestructive compared to DNA analysis methods [33,34]. Frank and Menz [35] utilized spectral data at different wavelengths to monitor the powdery mildew disease of leaf rust at different stages of development. Fungicide treatment was then applied using precision agriculture to determine the interaction of the crop with the fungicide. Results were compared with chemical analysis and showed an increase in early disease detection from 56% to 88.6%, which was considered an acceptable result for early disease detection. The goals of the present study were to: (i) determine the hyperspectral mean reflectance curves of Lw infested trees at different stages of development; (ii) select the optimal spectral bands for discrimination of damage due to Lw, Phytophthora root rot, and salinity.

2. Experimental Section

2.1. Host Plants and Inoculation in Greenhouse

Experiments were conducted in Miami-Dade County under an indoor controlled environment at the University of Florida's Tropical Research and Education Center (TREC) in Homestead, FL. Avocado leaves were obtained from the "Simmonds" variety of avocado trees which were grown in pots in greenhouse trials where different treatments were used to induce the certain symptoms and produce certain factors.

Avocado trees were one year old and almost 1 m tall. The pre-experiment methodology for each treatment is explained as follows:

Laurel wilt (Lw): Ten plants were inoculated with Lw at approximately 5 cm above the soil level by drilling four small holes around the circumference of the trunk. Each hole received 25 µL of a *R. lauricola* spore dilution at a concentration of 30,000 colony forming units (CFU)/mL for a total of 3000 CFU/plant. Holes were sealed with paraffin wrap. For the early inoculated stage of Lw, new

shoots were wilted and the leaf color changed from a dark oily green to light green on most leaves 14 days after inoculation (DAI), while others turned fully yellow. In that way, leaves were obtained 14 DAI for early stage and 45 DAI for late stage.

Salinity (Sln): One liter of salt solution was applied to each tree. The salt solution, at 36 g/L, was similar in concentration to that of the sea water from the east coast of Florida. Leaves showed some browning symptoms after seven days, and were taken for early stage. Then, another liter of the sea water liter was applied on experimental day 17. Further, browning symptoms were fully developed, similar to leaves affected by Lw after 21 days. Then, leaf samples representing salinity late stage were selected.

Phytophthora root rot (Prr): Ten plants were inoculated by infecting 10 pots with 6 grams of wheat seed colonized with *Phytophthora cinnamomi*. After 30 days, very few early symptoms of Prr appeared in the form of the yellowing of some leaves, and those leaves representing early stage were taken. After six months, late stage was considered for Phytophthora root rot and leaves were obtained.

Healthy (H): These plants were used as the control and were grown in full sun.

During the early growth stage, the plants showed few symptoms of Lw and Prr, so some leaves did not turn totally yellow, especially those infected with Prr. However, during the late growth stage the plants showed many symptoms of Lw and Sln, such as discoloration and necrotic leaves depending on the severity of the stress factor. Figure 1 shows tested avocado leaves during these two stages.

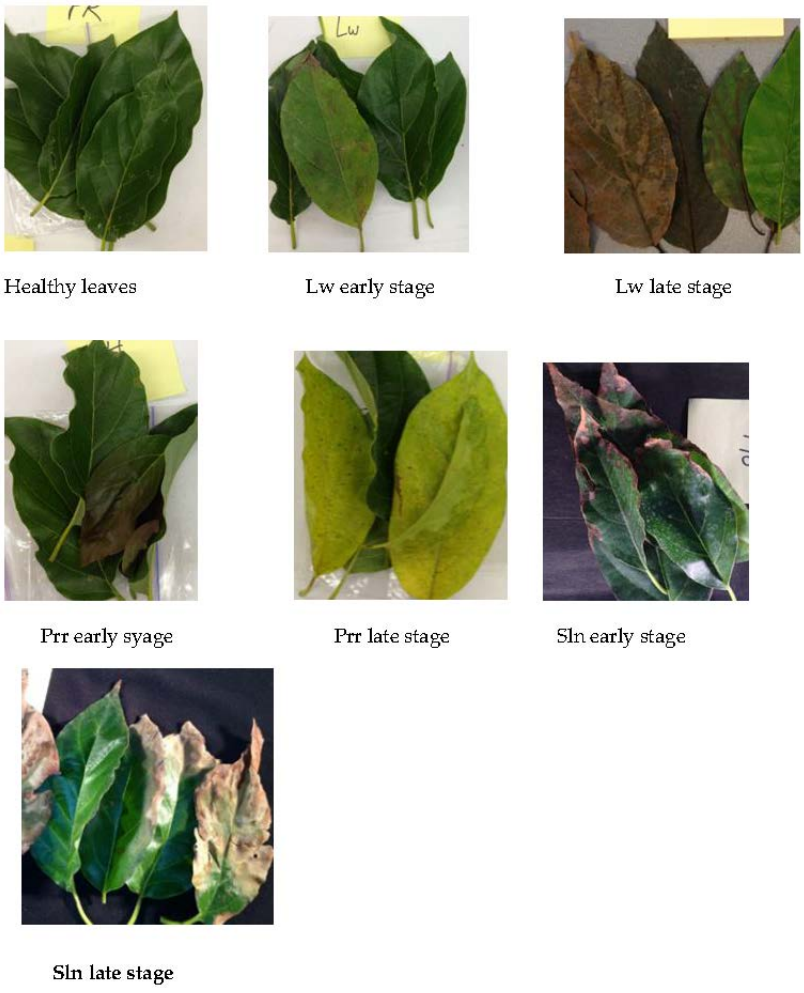

Figure 1. Avocado leaves in different stress stages: healthy, laurel wilt (Lw), Phytophthora root rot (Prr), and Salinity (Sln).

2.2. Spectral Data Collection

Forty leaves were sampled from each of the control and treated plants. Multiscans were taken at different positions in order to reduce the variability of the spectral device and the leaves. Five reflectance spectra per each leaf were collected at two stages of symptom development: early and late, depending on the symptomatic appearance. A handheld spectroradiometer (SVC HR-1024i™) (Spectra Vista Cooperation, Poughkeepsie, NY, USA) with a 4° field-of-view optical lens and a spectral range of 350 to 2500 nm was used. Two portable halogen work lamps (500 W) were used as the light source, and the reference reflectance spectra were acquired using a white reflectance reference panel (Spectralon Reflectance Target, CSTM-STR-99-100; Spectra Vista Cooperation) [1] (Figure 2). Spectral data were selected in the visible and near infrared domain from 350 to 950 nm. Spectral data were averaged for both stages to 10 nm and 40 nm based on previous studies [36,37]. The purpose of averaging data to 10 and 40 nm is to reduce the numerous wavelengths and also reduce noise and interference between wavebands. Additionally, waveband filters for 10 and 40 nm are available in the market and are reasonably priced for future sensor development. Therefore, the number of wavelengths for 456 nm was dropped to 49 and 15 wavelengths for 10 and 40 nm, respectively. Sample size for spectral reflectance data were applied between 196–200 for each category.

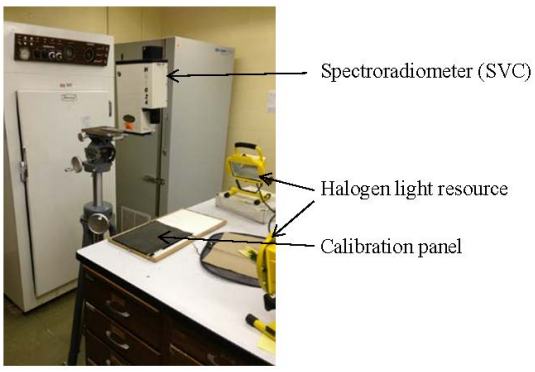

Figure 2. Laboratory set-up including spectroradiometer and halogen light sources.

2.3. Data Analysis and Classification

SPSS software (SPSS Statistics ver.13.0, IBM Corporation, Aramonk, NY, USA) was utilized in this study for spectral analysis. The classifications were between H, LW, Prr, and Sln based on the 10 nm and 40 nm averaged reflectance data. The classifications were conducted in two stages of disease development: early and late. The analyses were performed independently for the early and late stage spectral data, as well as in a data set composed of all of the reflectance data in order to select the best bands for each development stage.

2.3.1. Stepwise Discriminant Analysis

Discriminant analysis permits the setting up of a predictive model of group membership based on characteristics observed in each case [35]. This method determines significant differences between variables so that repetitive variables can be eliminated [38]. The stepwise discriminant analysis (STEPDISC) procedure combines forward selection and backward elimination of the variables; forward selection is employed for the inclusion of a variable, and backward elimination is used for the removal of variables no longer significant in the model [38]. A Wilks's lambda distribution was performed to determine the significance of each discriminant function; the lower the Wilks's lambda value, the greater the spectral differentiation between groups [39]. Thus, at each step, the variable that minimized the overall Wilks's lambda value was entered [35]. The data were randomized and separated into two independent parts: one was used to develop and construct the model and the second was used to validate the accuracy. The data set was divided into two parts: 30% for training and 70% for validation.

2.3.2. Neural Networks

Artificial neural networks operate by machine learning, in that inputs and outputs are given to the network one at a time and the network incrementally improves a model to approximate the input/output function [40]. Once the neural network has learned to carry out the desired function, the input values can be entered and the neural network will calculate the output [35]. Two neural networks were used: multilayer perceptron (MLP) and radial basis function (RBF).

The MLP neural model is a fully connected multilayer feed-forward supervised learning network trained by a back-propagation algorithm which reduces the quadratic error standard [35]. In the MLP, no values are fed back to earlier layers and the dimensions of the MLP are described as size of input layer × size of hidden layer × size of output layer [41,42]. In this study, the input layer was the spectral data of H, Lw, Prr, and Sln leaves. The RBF is also a fully connected feed-forward neural network with an input layer, a hidden layer, and an output layer [35]. The variables of the input and output layers were the same as those used in the MLP method. The main differences between these two neural networks are that in RBF, the associates between the input and output layers are not weighted and the transfer purposes on the hidden layer nodes are radially symmetric [43]. The capability of MLP and RBF for every classification model was determined by a hold-out cross-validation method. Cross validation consecutively classified all variables, but the first one to develop a classification function and then classify the variable was left out [44]. The full dataset was randomly split into three datasets by partitioning the active dataset into training 60%, testing 20%, and holdout 20% samples.

3. Results

Figure 3a–c show the spectral signature of the early and late stage disease development of Lw, Prr, and Sln as well as H, respectively. There are apparent reflectance differences in the red-edge and NIR regions for early and late stage development for all treatments. Higher differences are found between the late stage of each treatment and the control, suggesting the potential to discriminate disease or damage at that level of infection. Spectral signatures at the early stage are very similar to those of the control and doing more difficult to discriminate at that stage of development. In the late stage, external symptoms had developed, leaves were wilted or desiccated and were a dull gray-green or brown color while leaves in the early stage were still green and just beginning to lose turgidity.

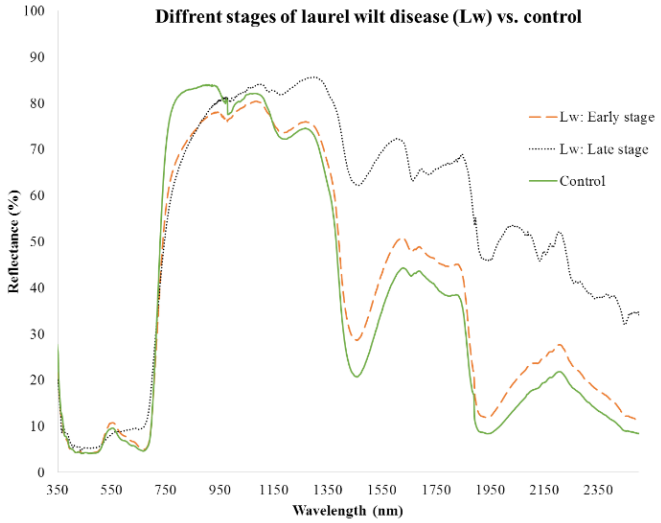

(**a**)

Figure 3. *Cont.*

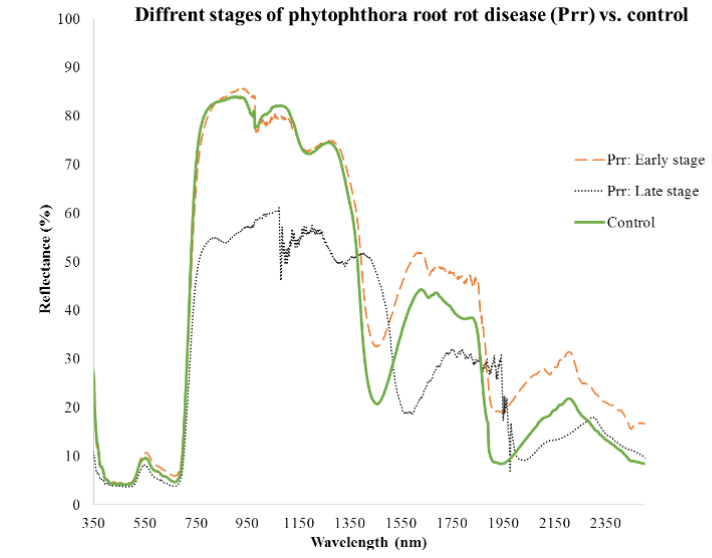

(**b**)

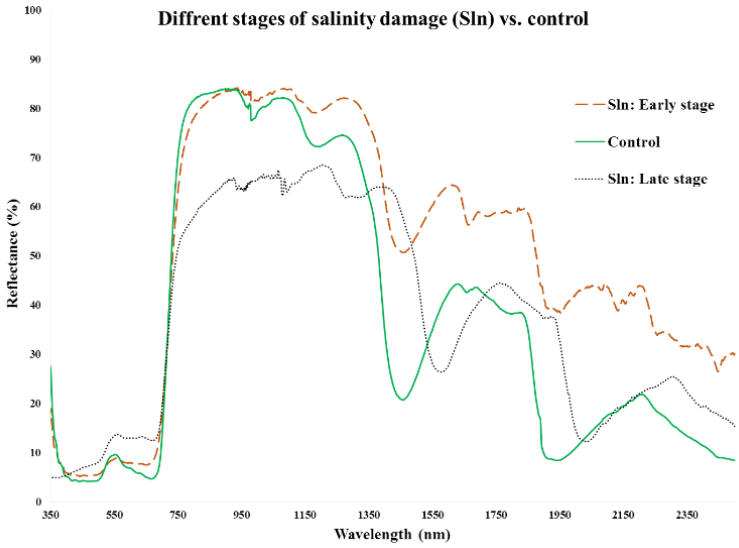

(**c**)

Figure 3. Spectral signature for laurel wilt disease (**a**); Phytophthora root rot (**b**); and salinity damage (**c**) in early and advanced stages vs. control.

3.1. Early Stage

In Figure 3c, the early stage of the Sln treatment shows higher reflectance values in the near infrared domain than for the late stage, which is typical for green vegetation. The same trend occurred for Lw and Prr diseases (Figure 3a,b). Figure 3b shows a similar spectral signature for H and Prr at the early stage, since after 14 days very few early symptoms of Prr appeared. Figure 3 also shows the reflectance of different bands for control, Lw, and Prr where it does not show a significant difference for spectral reflectance in the blue bands. On the other hand, Lw disease always exhibited lower reflectance in the NIR domain (750–950 nm) than H, Prr, and Sln.

Table 1 shows the classification results obtained from MLP and RBF for 10 nm and 40 nm bandwidth data, as well as the set of suitable wavelengths for that damaged and control leaf discrimination. The results obtained with MLP were better than those achieved with RBF where correct classification percentages ranged from 96% to 99% in all stages and comparisons (Table 1). RBF obtained the lowest classification rate (65%) for 10 nm at the early stage between H, Lw, and Sal.

Table 2 lists the percentage of correct classifications for every class in the MLP model at both the early and late stages for both studied bandwidths, 10 and 40 nm. In most of the cases, the obtained per class accuracy is around 100%, with the lowest value of 89% obtained for Sln class when the early stage dataset was used in the MLP analysis for the 40 nm bandwidth. These results prove that MLP allows for the classification that disease, since the probability that a classified pixel actually represents that category in reality is high enough. The confusion matrix analysis to determine the accuracy of the MLP method by comparing the percentage of classified pixels of H, Lw and Prr at early stage-10nm with the verified ground truth class, subsequently indicating the correct assessment, is shown in the Table 3.

Table 1. Hyperspectral classification of healthy (H), laurel wilt (Lw) disease, Phytophthora root rot (Prr), and salinity damage (Sln) in avocado and best wavebands selection using multilayer perceptron (MLP) and radial basis function (RBF) classification for different growth stages.

Stage and Parameter Setting	Importance Variable (nm)	Overall Classification (%)
Early stage 10 nm		
MLP: H, Lw, Sln	717, 750, 739, 526, 952, 772	**96**
MLP: H, Lw, Prr	750, 739, 952, 728, 717, 772	**96**
RBF: H, Lw, Sln	615, 627, 649, 660, 671,681	65
RBF: H, Lw, Prr	794, 806, 783, 817, 705, 693	71
Early stage 40 nm		
MLP: H, Lw, Sln	738, 780, 944, 615, 697, 656	**97**
MLP: H, Lw, Prr	491, 780, 697, 944, 615, 862	**97**
RBF: H, Lw, Sln	944, 697, 903, 615, 738, 862	73
RBF: H, Lw, Prr	409, 421, 433, 445, 457, 469	60
Late stage 10 nm		
MLP: H, Lw, Sln	885, 874, 952, 852, 841, 761	**99**
MLP: H, Lw, Prr	491, 780, 697, 944, 615, 862	**99**
RBF: H, Lw, Sal	761, 874, 885, 728, 952, 739	77
RBF: H, Lw, Prr	409, 421, 433, 445, 457, 469	97
Late stage 40 nm		
MLP: H, Lw, Sln	862, 780, 738, 944, 410, 903	**98**
MLP: H, Lw, Prr	862, 738, 410, 944, 697, 903	**97**
RBF: H, Lw, Sln	738, 944, 903, 410, 862, 697	77
RBF: H, Lw, Prr	410, 532, 450, 574, 862, 697	93

The values given in bold represent the overall accuracy best performance.

Table 2. Percentage of correct classification of early and late stage of healthy (H), laurel wilt (Lw), Phytophthora root rot (Prr) and salinity damage (Sln) using 10 and 40 nm bandwidth in the in the multilayer perceptron (MLP) model.

Data Set	Classes	Per Class Accuracy (%)				Overall Classification (%)
		H	Lw	Prr	Sln	
Early stage 10 nm	H, Lw, Prr	99	91	96	-	96
	H, Lw, Sln	100	91	-	97	96
Early stage 40 nm	H, Lw, Prr	95	98	98	-	97
	H, Lw, Sln	100	100	-	89	97
Late Stage10 nm	H, Lw, Prr	99	99	99	-	99
	H, Lw, Sln	100	100	-	98	99
Late stage 40 nm	H, Lw, Prr	98	96	98	-	97
	H, Lw, Sln	99	97	-	98	98

Table 3. Classification matrix obtained from the multilayer perceptron (MLP) neural network (for 2010) using 10 bandwidth data and healthy (H), laurel wilt (Lw), Phytophthora root rot (Prr) early stage.

Observed Spectra	Predicted Spectra			Per Class Accuracy
	H	Lw	Sln	
H	30	3	0	99.1%
Lw	0	39	0	90.9%
Sln	0	2	44	100%
	Overall classification			95.8%

Table 4 shows the classification results for STEPDISC analysis and the bands that were chosen on the basis of their order of entry into the STEPDISC procedure selection to discriminate between H, Lw, Sln, and Prr leaves at early and late stages. The most frequently selected wavelengths were found in the red-edge range (717–750 nm) for the 10 nm bandwidth and in the red-edge and blue ranges for 40 nm. In each of the cases studied, a small Wilks's lambda (0.0–0.2) was obtained indicating the high discriminatory power of every set of selected wavebands.

Table 4. Hyperspectral classification of laurel wilt (Lw), Healthy (H), Phytophthora root rot (Prr), and salinity damage (Sln) and the best wavebands selection using stepwise discriminant (STEPDISC) analysis for different growth stages.

Stage-Waveband Input Data	Best Bands Selected	Wilks's Lambda	Cross Validation
Early stage-10 nm			
H, Lw, Prr	806, 761, 548, 638, 885, 941, 537	0.2	82%
H, Lw, Sln	908, 745, 852, 504, 445, 638, 604	0.2	86%
Early stage-40 nm			
H, Lw, Prr	618, 781, 822, 904, 657, 575, 410, 740, 451, 945, 493	0.2	83%
H, Lw, Sln	595, 904, 781, 410, 534, 740, 698, 657, 616, 493	0.2	82%
Late stage-10 nm			
H, Lw, Prr	817, 829, 761, 409, 941, 548, 560, 421	0.0	98%
H, Lw, Sln	560, 761, 806, 750, 885, 829, 409, 421, 504, 593, 515	0.05	92%
Late stage-40 nm			
H, Lw, Prr	817, 829, 761, 409, 941, 548, 560, 421	0.0	98%
H, Lw, Sln	560, 761, 806, 750, 885, 829, 409, 421, 504, 593, 515	0.05	92%

3.2. Late Stage

The development stages of Lw disease varied in the visible and NIR ranges. The late stages had high reflectance in the 1300–2500 nm range. The late developmental stage showed a lower reflectance in the NIR range of 700–950 nm. Reflectance curves for plants affected by Sln varied from stage to stage depending on salinity concentration. Figure 3a shows Lw's spectral reflectance in the visible range from 550 to 700 nm increased during the late stage. Lw's late stage showed a significant difference in spectral reflectance spectra for healthy plants. The Prr late stage displayed lower reflectance than that of the healthy plants (Figure 3b). The spectral signature curve showed variation in reflectance values, especially for Prr late stages in the NIR domain. The overall classification percentage was 92%–99% for all MLP. STEPDISC was the second-best method with RBF being the worst of the three classification methods.

3.3. Combination of Early and Late Stages

Table 5 shows the MLP and RBF classification results for the combination of the early and late growth stages for the 10 and 40 nm bandwidths. RBF produced a low value and a high value of

classification for the combination of H, Lw, and Prr for 40 and 10 nm (65% and 71%, respectively). MLP resulted in a high classification value for the combination of H, Lw, and Prr at 10 nm, while the combinations of H, Lw, and Sal at 40 nm and H, Lw, and Prr at 40 nm had the lowest value. NIR (700–900 nm) was the most frequent range, especially the red-edge, with the exception of the combination of H, Lw, and Prr at 10 nm under MLP for which the blue and green bands were the most common (445, 515, 504, 433 nm). Stepwise classification values are shown in Table 6. The lowest classification in Table 6 is that of the combination of H, Lw, and Sal at 40 nm having a cross validation value of 80%. The average of all categories at 10 nm had a higher value than the average of the categories at 40 nm. The wavebands between 700–800 nm were the most common for all categories. The correct classification percentage was 92%–98% for all MLP. STEPDISC was the second best method, with RBF being the worst of the three classification methods.

Table 5. Reflectance classification using MLP and RBF methods for laurel wilt (Lw), Healthy (H), Phytophthora root rot (Prr), and salinity damage (Sal) in early and late stage combined.

Stage and Parameter Settings	Neural Network	Importance Wavebands (nm)	Overall Classification
H, Lw, Sal, 10 nm	MLP	750, 717, 433, 705, 772, 693, 604	94%
H, Lw, Sal, 10 nm	RBF	705, 537, 548, 409, 717, 560, 526, 941, 952, 433, 615	67%
H, Lw, Prr, 10 nm	MLP	445, 515, 504, 433, 638, 705, 750, 817, 421, 739, 952, 493, 615, 761, 604	98%
H, Lw, Prr, 10 nm	RBF	671, 681, 660, 649, 638, 693, 627	71%
H, Lw, Sal, 40 nm	MLP	738, 780, 944, 862, 903, 450	93%
H, Lw, Sal, 40 nm	RBF	944, 903, 862, 738, 656, 532, 450, 820, 491, 615, 574, 410, 780, 697	70%
H, Lw, Prr, 40 nm	MLP	944, 821, 656, 862	93%
H, Lw, Prr, 40 nm	RBF	944, 697, 903, 532, 738, 656, 574, 615, 862, 780, 821, 410	65%

Table 6. Classification reflectance result using STEPDISC for H, Lw, salinity, and Prr in early and late stage combined.

Input Data	Best Bands Selected (nm)	Wilk's Lambda	Cross Validation
H, Lw, Sln: 10 nm	772, 794, 504, 548, 705, 638, 693, 681, 604, 717, 615, 445	0.0	87%
H, Lw, Prr: 10 nm	750, 885, 829, 952, 548, 649, 693, 638, 705, 537, 515, 681	0.06	89%
H, Lw, Sln: 40 nm	780, 820, 491, 532, 944, 410, 574, 697, 450, 656	0.05	80%
H, Lw, Prr: 40 nm	780, 862, 944, 532, 574, 738, 697, 656, 410, 450, 615	0.03	81%

4. Discussion

In the early stage for Lw and all other stress factors, the spectral reflectance showed varying reflectance signatures, for example, in the visible range the spectral signature increased in the blue and red range while in the green range, it showed either an increase or a decrease of reflectance value. Although we were able to observe the changing of the colors of the leaves for many of the categories, not all had the same level of change. The challenge was for trees that were in the very early stage "asymptomatic". At this stage, it was not easy to differentiate between healthy and infected trees. The chlorophyll and pigment in leaves strongly absorb blue and red light in order to conduct the photosynthesis that is necessary for plant metabolism, meaning that any change in concentration of the chlorophyll will lead to changes in spectral reflectance depending on the pigment ratio [45,46]. NIR domain reflectance can provide good indicators of cell structure damage to leaves caused by disease, drought, and nutrient deficiency. Any overall change in the leaf will impact the spectral reflectance

which therefore makes it a good indicator to use in hyperspectral detection methods [25,47]. The spectral signature for healthy plants had high absorption in red and blue, with a green peak at 550 nm. Each disease development stage had unique spectral reflectance signatures, indicating a relationship between spectral signature and the appearance of disease symptoms [27,28].

In the NIR domain, the reflectance increased or decreased depending on the disease symptom stage, thus leaf cell damage for Lw, Sln, and Prr showed different reflectance curves than for the healthy plant. Water content is another factor that might have an effect on reflectance. Water content could affect the absorbance or reflectance of light depending on the water quantity in the leaf [48–51]. The ambrosia beetle blocks the flow of water in the xylem to support its growth, and therefore water flow or water content is a very important indicator for this disease. All of these factors (e.g., chlorophyll concentration, water content, wall cell damage, and severity of disease) could affect spectral signature and showed different curve signatures. Each affecting factor has a different curve signature for all categories [24–26].

The main purpose of this study was to select spectral bands in the VIS-NIR range that can be used to differentiate between healthy, laurel wilt diseased, salinity damaged, and Phytophthora root rot infested trees. Several wavebands were selected for classifying trees with different stages and types of disease and stress factors. There are many studies on band selection to obtain the best bands in the VIS-NIR range to reduce the huge number of narrow bands, minimize redundancy, and to obtain a statistical model without a long process (i.e., smaller number of spectral bands are more convenient and more efficient in hyperspectral analysis) [48,52–55]. The MLP classification method resulted in classification values for all of these treatments. This is related to the progressive nature of disease development, which makes it easier to differentiate the late stage than the early stage. By detecting disease at the early stage, particularly at asymptomatic stage, growers can spray or remove the affected tree and manage the disease more cost effectively before the disease spreads to the rest of the grove [36]. Using smaller number of spectral bands it is possible to use inexpensive remote sensing tools such as small drones to detect the LW infected trees [36]. The results of this study agree with the results of other studies using classification methods [35], so the classification accuracy were higher in late stage of infection compare to the other stage of the disease. The purpose of combining the early stage and late stage data to obtain wavebands could be used in the early and late stage at the same time because not all tree leaves show a lot of symptoms at the same time. Disease is transmitted depending on severity of disease and disease development stage [24,37]. Environmental factors and the population of the vectors also affect the dynamic disease transmission in plants [14,56,57]. Sometimes the symptoms would be obvious in the crown and do not appear on the bottom side of the tree. Fast decision-making and time-effective spraying at specific locations will lead to less pollution of the environment. Accurate band selection and classification are important to encourage the grower to use these methods for timely and appropriate decision-making. This is the first instance in which the spectral signatures of leaves from avocado trees have been used to determine spectral reflectance and to recommend appropriate bands to detect Lw disease and other factors.

5. Conclusions

The results of this study showed that it is possible to classify Lw-, Phytophthora root rot-, and salinity-damaged leaves of avocado trees from healthy leaves using visible and near-infrared (400–950 nm) spectral bands for the data collected under laboratory conditions. The classification of different diseases and stress factors studied in this work can be done at both the early and the late stage of disease infection; however, developing a classification technique that works for both early and late stage of different diseases and stress factors will result in lower detection accuracy. Since for practical purposes, it is more desirable to detect the disease at the early stage of disease or stress infection, it is better to use a classification model that is developed for early stage. Comparing the classification results for 10-nm and 40-nm bandwidths showed similar results, indicating that the narrower band width does not produce better results and that the 40 nm wide bands can be as good as

narrower bands. The MLP model created the best classification accuracy in both early and late stage as compared to other models used in this study. The next step of this study is to test this model under field conditions in commercial groves to test the validity of the model under field conditions.

Acknowledgments: The author would like to thank the Florida Dept. of Agriculture and Consumer Services, USDA Specialty Block Grant No. 019730 for partially funding this study and the Ministry of Higher Education and Scientific Research of Republic of Iraq for supporting the graduate student working on this project. We would also like to thank Dr. Randy Ploetz and Mr. Joshua Konkol at the Tropical Research and Education Center in Homestead for providing us the stressed and diseased plants; and Sherrie Buchanonand and Cininta Pertiwi for assisting with the data collections.

Author Contributions: All authors contributed equally to the paper.

Conflicts of Interest: The authors declare no conflict of interest.

References

1. United States Department of Agriculture (USDA). Noncitrus Fruits and Nuts: 2008 Preliminary Summary. Available online: http://usda.mannlib.cornell.edu/usda/nass/NoncFruiNu//2000s/2009/NoncFruiNu-01-23-2009_revision.pdf (accessed on 18 August 2016).
2. Evans, E.A.; Crane, J.; Hodges, A.; Osborne, J.L. Potential economic impact of laurel wilt disease on the Florida avocado industry. *Horttechnology* **2010**, *20*, 234–238.
3. Evans, E.A. Sample avocado production costs and profitability analysis for Florida. In *Electronic Data Information Source (EDIS) FE 837*; Bernal Lozano, I., Ed.; Food and Resource Economics Department, University of Florida: Gainesville, FL, USA, 2015.
4. Evans, J.P.; Scheffers, B.R.; Hess, M. Effect of laurel wilt invasion on redbay populations in a maritime forest community. *Biol. Invasions* **2014**, *16*, 1581–1588. [CrossRef]
5. Carrillo, D.; Crane, J.H.; Pena, J.E. Potential of contact insecticides to control *Xyleborus glabratus* (Coleoptera: Curculionidae), a vector of laurel wilt disease in avocados. *J. Econ. Entomol.* **2013**, *106*, 2286–2295. [CrossRef] [PubMed]
6. Ploetz, R.; Schaffer, B.; Vargas, A.; Konkol, J.; Salvatierra, J.; Inch, S.; Campbell, A.; Wideman, R. Physiological impacts of laurel wilt on avocado. *Phytopathology* **2013**, *103*, 114.
7. Kendra, P.E.; Montgomery, W.S.; Niogret, J.; Pruett, G.E.; Mayfield, A.E., 3rd; MacKenzie, M.; Deyrup, M.A.; Bauchan, G.R.; Ploetz, R.C.; Epsky, N.D. North American Lauraceae: Terpenoid emissions, relative attraction and boring preferences of redbay ambrosia beetle, *Xyleborus glabratus* (Coleoptera: Curculionidae: Scolytinae). *PLoS ONE* **2014**, *9*, e102086. [CrossRef] [PubMed]
8. Kuhns, E.H.; Martini, X.; Tribuiani, Y.; Coy, M.; Gibbard, C.; Pena, J.; Hulcr, J.; Stelinski, L.L. Eucalyptol is an attractant of the redbay ambrosia beetle, *Xyleborus glabratus*. *J. Chem. Ecol.* **2014**, *40*, 355–362. [CrossRef] [PubMed]
9. Fraedrich, S.W.; Harrington, T.C.; Rabaglia, R.J.; Ulyshen, M.D.; Mayfield, A.E., III; Hanula, J.L.; Eickwort, J.M.; Miller, D.R. A fungal symbiont of the redbay ambrosia beetle causes a lethal wilt in redbay and other Lauraceae in the southeastern United States. *Plant Dis.* **2008**, *92*, 215–224. [CrossRef]
10. Hanula, J.L.; Mayfield, A.E., III; Fraedrich, S.W.; Rabaglia, R.J. Biology and host associations of redbay ambrosia beetle (Coleoptera: Curculionidae: Scolytinae), exotic vector of laurel wilt killing redbay trees in the southeastern United States. *J. Econ. Entomol.* **2008**, *101*, 1276–1286. [CrossRef] [PubMed]
11. Kendra, P.E.; Montgomery, W.S.; Niogret, J.; Epsky, N.D. An uncertain future for American Lauraceae: A lethal threat from redbay ambrosia beetle and laurel wilt disease (a review). *Am. J. Plant Sci.* **2013**, *4*, 727–738. [CrossRef]
12. Carrillo, D.; Duncan, R.E.; Pena, J.E. Ambrosia beetles (Coleoptera: Curculionidae: Scolytinae) that breed in avocado wood in florida. *Fla. Entomol.* **2012**, *95*, 573–579. [CrossRef]
13. Jeyaprakash, A.; Davison, D.A.; Schubert, T.S. Molecular detection of the laurel wilt fungus, Raffaelea lauricola. *Plant Dis.* **2014**, *98*, 559–564. [CrossRef]
14. Ploetz, R.C.; Perez-Martinez, J.M.; Smith, J.A.; Hughes, M.; Dreaden, T.; Blanchette, R.; Held, B.; Inch, S.A. Laurel Wilt: A dangerous new disease of avocado in the Western Hemisphere. In Proceedings of the Caribbean Food Crops Society 46th Annual Meeting and T-Star Invasive Symposium, Boca Chica, Dominican Republic, 11–17 July 2010; pp. 97–106.

15. Sankaran, S.; Ehsani, R.; Inch, S.A.; Ploetz, R.C. Evaluation of visible-near infrared reflectance spectra of avocado leaves as a non-destructive sensing tool for detection of laurel wilt. *Plant Dis.* **2012**, *96*, 1683–1689. [CrossRef]
16. Ploetz, R.C.; Perez-Martinez, J.M.; Smith, J.A.; Hughes, M.; Dreaden, T.J.; Inch, S.A.; Fu, Y. Responses of avocado to laurel wilt, caused by Raffaelea lauricola. *Plant Pathol.* **2012**, *61*, 801–808. [CrossRef]
17. Inch, S.A.; Ploetz, R.C. Impact of laurel wilt, caused by *Raffaelea lauricola*, on xylem function in avocado, *Persea americana*. *For. Pathol.* **2012**, *42*, 239–245. [CrossRef]
18. Sankaran, S.; Ehsani, R.; Etxeberria, E. Mid-infrared spectroscopy for detection of Huanglongbing (greening) in citrus leaves. *Talanta* **2010**, *83*, 574–581. [CrossRef] [PubMed]
19. Henson, J.M.; French, R. The polymerase chain reaction and plant disease diagnosis. *Annu. Rev. Phytopathol.* **1993**, *31*, 81–109. [CrossRef] [PubMed]
20. Bravo, C.; Moshou, D.; West, J.; McCartney, A.; Ramon, H. Early disease detection in wheat fields using spectral reflectance. *Biosyst. Eng.* **2003**, *84*, 137–145. [CrossRef]
21. Graeff, S.; Claupein, W. Quantifying nitrogen status of corn (*Zea mays* L.) in the field by reflectance measurements. *Eur. J. Agron.* **2003**, *19*, 611–618. [CrossRef]
22. Curran, P. Introduction to environmental remote sensing (fourth edition). *Geography* **2000**, *85*, 376.
23. Hunsche, M.; Buerling, K.; Noga, G. Spectral and time-resolved fluorescence signature of four weed species as affected by selected herbicides. *Pestic. Biochem. Physiol.* **2011**, *101*, 39–47. [CrossRef]
24. Blackburn, G.A. Spectral indices for estimating photosynthetic pigment concentrations: A test using senescent tree leaves. *Int. J. Remote Sens.* **1998**, *19*, 657–675. [CrossRef]
25. Broge, N.H.; Leblanc, E. Comparing prediction power and stability of broadband and hyperspectral vegetation indices for estimation of green leaf area index and canopy chlorophyll density. *Remote Sens Environ.* **2001**, *76*, 156–172. [CrossRef]
26. Abdulridha, J.; de Castro, A.; Ehsani, R. Differentiate Laurel wilt disease and nutrient deficiency in avocado trees using Vis–NIR spectroscopy. In Proceedings of the 2015 ASABE Annual International Meeting, New Orleans, LA, USA, 26–29 July 2015.
27. Moran, M.S.; Inoue, Y.; Barnes, E.M. Opportunities and limitations for image-based remote sensing in precision crop management. *Remote Sens. Environ.* **1997**, *61*, 319–346. [CrossRef]
28. Pinter, P.J.; Hatfield, J.L.; Schepers, J.S.; Barnes, E.M.; Moran, M.S.; Daughtry, C.S.T.; Upchurchm, D.R. Remote sensing for crop management. *Photogramm. Eng. Remote Sens.* **2003**, *69*, 647–664. [CrossRef]
29. Vrindts, E.; De Baerdemaeker, J.; Ramon, H. Weed detection using canopy reflection. *Precis. Agric.* **2002**, *3*, 63–80. [CrossRef]
30. Mahlein, A.K.; Steiner, U.; Dehne, H.W.; Oerke, E.C. Spectral signatures of sugar beet leaves for the detection and differentiation of diseases. *Precis. Agric.* **2010**, *11*, 413–431. [CrossRef]
31. Rumpf, T.; Mahlein, A.K.; Steiner, U.; Oerke, E.C.; Dehne, H.W.; Pluemer, L. Early detection and classification of plant diseases with Support Vector Machines based on hyperspectral reflectance. *Comput. Electron. Agric.* **2010**, *74*, 91–99. [CrossRef]
32. Ma, R.; Yang, B.; Zhang, L.; Liu, Z. Design and implementation of a forest fire monitoring system using a miniature unmanned aerial vehicle. *J. Zhejiang A F Univ.* **2012**, *29*, 783–789.
33. Menesatti, P.; Antonucci, F.; Pallottino, F.; Roccuzzo, G.; Allegra, M.; Stagno, F.; Intrigliolo, F. Estimation of plant nutritional status by Vis–NIR spectrophotometric analysis on orange leaves *Citrus sinensis* (L) Osbeck *cv* Tarocco. *Biosyst. Eng.* **2010**, *105*, 448–454. [CrossRef]
34. Tomkiewicz, D.; Piskier, T. A plant based sensing method for nutrition stress monitoring. *Precis. Agric.* **2012**, *13*, 370–383. [CrossRef]
35. Franke, J.; Menz, G. Multi-temporal wheat disease detection by multi-spectral remote sensing. *Precis. Agric.* **2007**, *8*, 161–172. [CrossRef]
36. De Castro, A.; Ehsani, R.; Ploetz, R.; Crane, J.; Abdulridha, J. Optimum spectral and geometric parameters for early detection of laurel wilt disease in avocado. *Remote Sens. Environ.* **2015**, *171*, 33–44. [CrossRef]
37. Pant, P.; Heikkinen, V.; Korpela, I.; Hauta-Kasari, M.; Tokola, T. Logistic regression-based spectral band selection for tree species classification: Effects of spatial scale and balance in training samples. *IEEE Geosci. Remote Sens. Lett.* **2014**, *11*, 1604–1608. [CrossRef]

38. De Castro, A.I.; Jurado-Exposito, M.; Gomez-Casero, M.T.; Lopez-Granados, F. Applying neural networks to hyperspectral and multispectral field data for discrimination of cruciferous weeds in winter crops. *Sci. World J.* **2012**, *2012*, 630390. [CrossRef] [PubMed]
39. Karimi, Y.; Prasher, S.O.; McNairn, H.; Bonnell, R.B.; Dutilleul, P.; Goel, P.K. Discriminant analysis of hyperspectral data for assessing water and nitrogen stresses in corn. *Trans. ASAE* **2005**, *48*, 805–813. [CrossRef]
40. Thenkabail, P.S.; Gamage, M.; Smakhtin, V.U. *The Use of Remote Sensing Data for Drought Assessment and Monitoring in Southwest Asia*; Research Report; International Water Management Institute: Colombo, Sri Lanka, 2005.
41. Park, J.; Sandberg, I.W. Approximation and radial-basis-function networks. *Neural Comput.* **1993**, *5*, 305–316. [CrossRef]
42. Keranen, M.; Aro, E.M.; Tyystjarvi, E.; Nevalainen, O. Automatic plant identification with chlorophyll fluorescence fingerprinting. *Precis. Agric.* **2003**, *4*, 53–67. [CrossRef]
43. Jayawardena, A.W.; Fernando, D.K.; Zhou, M.C. Comparison of multilayer perceptron and radial basis function network as flood forecasting. *IAHS* **1997**, *239*, 173–182.
44. Burks, T.F.; Shearer, S.A.; Heath, J.R.; Donohue, K.D. Evaluation of neural-network classifiers for weed species discrimination. *Biosyst. Eng.* **2005**, *91*, 293–304. [CrossRef]
45. Chernick, M.R.; Murthy, V.K.; Nealy, C.D. Estimation of error rate for linear discriminant functions by resampling—Non-Gaussian populations. *Comput. Math. Appl.* **1988**, *15*, 29–37. [CrossRef]
46. Carter, G.A.; Knapp, A.K. Leaf optical properties in higher plants: Linking spectral characteristics to stress and chlorophyll concentration. *Am. J. Bot.* **2001**, *88*, 677–684. [CrossRef] [PubMed]
47. West, J.S.; Bravo, C.; Oberti, R.; Lemaire, D.; Moshou, D.; McCartney, H.A. The potential of optical canopy measurement for targeted control of field crop diseases. *Annu. Rev. Phytopathol.* **2003**, *41*, 593–614. [CrossRef] [PubMed]
48. Wang, F.M.; Huang, J.F.; Xu, J.F.; Wang, X.Z. Wavebands selection tor rice information extraction based on spectral bands inter-correlation. *Spectrosc. Spectr. Anal.* **2008**, *28*, 1098–1101.
49. Sims, D.A.; Gamon, J.A. Relationships between leaf pigment content and spectral reflectance across a wide range of species, leaf structures and developmental stages. *Remote Sens. Environ.* **2002**, *81*, 337–354. [CrossRef]
50. Sims, D.A.; Gamon, J.A. Estimation of vegetation water content and photosynthetic tissue area from spectral reflectance: A comparison of indices based on liquid water and chlorophyll absorption features. *Remote Sens. Environ.* **2003**, *84*, 526–537. [CrossRef]
51. Carter, G.A. Primary and secondary effects of water-content on the spectral reflectance of leaves. *Am. J. Bot.* **1991**, *78*, 916–924. [CrossRef]
52. Gamon, J.A.; Surfus, J.S. Assessing leaf pigment content and activity with a reflectometer. *New Phytol.* **1999**, *143*, 105–117. [CrossRef]
53. Chang, C.I.; Liu, K.H. Progressive band selection of spectral unmixing for hyperspectral imagery. *IEEE Trans. Geosci. Remote Sens.* **2014**, *52*, 2002–2017. [CrossRef]
54. Gomez-Casero, M.T.; Castillejo-Gonzalez, I.L.; Garcia-Ferrer, A.; Pena-Barragan, J.M.; Jurado-Exposito, M.; Garcia-Torres, L.; López-Granados, F. Spectral discrimination of wild oat and canary grass in wheat fields for less herbicide application. *Agron. Sustain. Dev.* **2010**, *30*, 689–699. [CrossRef]
55. Li, S.; Qiu, J.; Yang, X.; Liu, H.; Wan, D.; Zhu, Y. A novel approach to hyperspectral band selection based on spectral shape similarity analysis and fast branch and bound search. *Eng. Appl. Artif. Intell.* **2014**, *27*, 241–250. [CrossRef]
56. Sankaran, S.; Ehsani, R. Detection of huanglongbing disease in citrus using fluorescence spectroscopy. *Trans. ASABE* **2012**, *55*, 313–320. [CrossRef]
57. Garrett, K.A.; Dendy, S.P.; Frank, E.E.; Rouse, M.N.; Travers, S.E. Climate change effects on plant disease: Genomes to ecosystems. *Annu. Rev. Phytopathol.* **2006**, *44*, 489–509. [CrossRef] [PubMed]

© 2016 by the authors; licensee MDPI, Basel, Switzerland. This article is an open access article distributed under the terms and conditions of the Creative Commons Attribution (CC-BY) license (http://creativecommons.org/licenses/by/4.0/).